Characterisation of the p53 pathway in cell lines established from TH-*MYCN* transgenic mouse tumours

LINDI CHEN[1], ARMAN ESFANDIARI[2], WILLIAM REAVES[1], ANNETTE VU[3], MICHAEL D. HOGARTY[3], JOHN LUNEC[2] and DEBORAH A. TWEDDLE[1]

[1]Wolfson Childhood Cancer Research Centre and [2]Newcastle Cancer Centre, Northern Institute for Cancer Research, Newcastle University, Newcastle upon Tyne NE1 7RU, UK; [3]The Children's Hospital of Philadelphia, University of Pennsylvania Perelman School of Medicine, Philadelphia, PA 19104, USA

Received August 17, 2017; Accepted December 12, 2017

DOI: 10.3892/ijo.2018.4261

Abstract. Cell lines established from the TH-*MYCN* transgenic murine model of neuroblastoma are a valuable preclinical, immunocompetent, syngeneic model of neuroblastoma, for which knowledge of their p53 pathway status is important. In this study, the *Trp53* status and functional response to Nutlin-3 and ionising radiation (IR) were determined in 6 adherent TH-*MYCN* transgenic cell lines using Sanger sequencing, western blot analysis and flow cytometry. Sensitivity to structurally diverse MDM2 inhibitors (Nutlin-3, MI-63, RG7388 and NDD0005) was determined using XTT proliferation assays. In total, 2/6 cell lines were *Trp53* homozygous mutant (NHO2A and $844^{MYCN+/+}$) and 1/6 ($282^{MYCN+/-}$) was *Trp53* heterozygous mutant. For 1/6 cell lines (NHO2A), DNA from the corresponding primary tumour was found to be *Trp53* wt. In all cases, the presence of a mutation was consistent with aberrant p53 signalling in response to Nutlin-3 and IR. In comparison to *TP53* wt human neuroblastoma cells, *Trp53* wt murine control and TH-*MYCN* cell lines were significantly less sensitive to growth inhibition mediated by MI-63 and RG7388. These murine *Trp53* wt and mutant TH-*MYCN* cell lines are useful syngeneic, immunocompetent neuroblastoma models, the former to test p53-dependent therapies in combination with immunotherapies, such as anti-GD_2, and the latter as models of chemoresistant relapsed neuroblastoma when aberrations in the p53 pathway are more common. The spontaneous development of *Trp53* mutations in 3 cell lines from TH-*MYCN* mice may have arisen from *MYCN* oncogenic driven and/or *ex vivo* selection. The identified species-dependent selectivity of MI-63 and RG7388 should be considered when interpreting *in vivo* toxicity studies of MDM2 inhibitors.

Correspondence to: Professor Deborah A. Tweddle, Wolfson Childhood Cancer Research Centre, Northern Institute for Cancer Research, Newcastle University, Level 6 Herschel Building, Brewery Lane, Newcastle upon Tyne, NE1 7RU, UK
E-mail: deborah.tweddle@ncl.ac.uk

Abbreviations: IR, ionising radiation; wt, wild-type; PBS, phosphate-buffered saline; FCS, fetal calf serum

Key words: neuroblastoma, TH-MYCN, p53 pathway, MDM2 inhibitors, Nutlin-3, RG7388, MI-63, NDD0005

Introduction

Neuroblastoma, an embryonal malignancy of the developing sympathetic nervous system, remains one of the most difficult paediatric cancers to cure with <50% of high-risk patients being long-term survivors despite intensive multi-modal therapy. *MYCN* amplification occurs in ~50% of high-risk cases, associated with rapid tumour progression and a poor prognosis (1). The role of MYCN in neuroblastoma tumourigenesis has been demonstrated by the generation of TH-*MYCN* transgenic mice in 1997 through the transfer of a construct incorporating human *MYCN* cDNA under the control of the rat tyrosine hydroxylase promoter into the nucleus of fertilised murine oocytes and subsequent integration into genomic DNA (2,3). The tyrosine hydroxylase promoter leads to tissue-targeted overexpression of human *MYCN* in neural crest cells, and mice develop spontaneous highly penetrant abdominal and para-spinal thoracic tumours consistent with sites of human neuroblastoma (2). Tumour penetrance and growth have been shown to be related to *MYCN* gene dosage where homozygotes develop tumours with increased incidence and decreased latency (2,4). Analysis of TH-*MYCN* tumours has shown that they recapitulate many histological features of human neuroblastoma with varying degrees of neuronal differentiation and express synaptophysin and neuron-specific enolase (2). Moreover, tumours also exhibit chromosomal changes syntenic with those observed in human neuroblastoma tumours, such as gain of chromosome 17 (2,4). The TH-*MYCN* transgenic mouse is now a well-established model of neuroblastoma, and a panel of homozygous and hemizygous TH-*MYCN* cell lines have been derived from tumour resections from these mice, similarly reflecting both the genetic and biological features of human neuroblastoma (5). Although micrometastases can occur, one major limitation of the TH-*MYCN* transgenic model in preclinical drug development studies is the very low incidence of clinically relevant metastases to sites such as bone marrow, thus limiting its usefulness as a model for high-risk metastatic neuroblastoma (6). To overcome this, TH-*MYCN* cell lines

have been used to generate highly valuable orthotopic and pseudometastatic syngeneic models of neuroblastoma in an immunocompetent background (7,8). This is of particular importance as immunotherapies, such as anti-GD_2 antibody are currently standard of care for the treatment of children with high-risk neuroblastoma.

The tumour suppressor gene, *TP53*, is critical in maintaining genomic stability and is mutationally inactivated in >50% of all human malignancies (9). Abnormalities in the p53 pathway can contribute to tumour resistance against ionising radiation (IR) and cytotoxic chemotherapies (10-13). In neuroblastoma tumours and cell lines established at diagnosis, *TP53* mutations are rare; however an increased frequency of mutations has been reported at relapse/post-chemotherapy (14-16). Knowledge of *Trp53* genetic and functional status in TH-*MYCN* cell lines is important if they are to be used in preclinical syngeneic neuroblastoma models.

In this study, we characterised the genetic and functional status of p53 in 6 adherent TH-*MYCN* transgenic murine cell lines, and demonstrate that 3/6 cell lines have *Trp53* mutations and could be used to generate valuable syngeneic models of p53 non-functional relapsed neuroblastoma. Moreover, we provide evidence of the species-dependent selectivity of some MDM2 inhibitors, which should be considered when selecting murine models for preclinical toxicity testing of MDM2 inhibitors.

Materials and methods

Cell lines. The TH-*MYCN* transgenic murine cell lines used were MYCN homozygous NHO2A, $844^{MYCN+/+}$, $3261^{MYCN+/+}$, $3394^{MYCN+/+}$, $3399^{MYCN+/+}$ and hemizygous $282^{MYCN+/-}$. The NHO2A cell line has been previously described (5) and together with NHO2A mouse tumour DNA, was obtained from Professor Michelle Haber (Children's Cancer Institute, Sydney, NSW, Australia). All other previously unreported TH-*MYCN* cell lines were established from the TH-*MYCN* colony at the Children's Hospital of Philadelphia (Philadelphia, PA, USA) under an IACUC approved animal protocol. Genetically-engineered 129X1/SvJ mice carrying the TH-*MYCN* transgene in one concatamer (TH-$MYCN^{+/-}$ mice) or two concatamers (TH-$MYCN^{+/+}$ mice) develop tumours closely resembling human neuroblastoma (2). TH-$MYCN^{+/-}$ mice were bred and offspring genotyped as described previously (17). TH-*MYCN* mice were euthanised at the time of tumour progression according to humane approved guidelines using 3-5% isoflurane inhalation followed by cervical dislocation. The mice were then disinfected with 70% ethanol prior to resecting the tumour free. Tumours were fragmented and filtered through a 40 μm nylon mesh filter into a conical tube, spun-pelleted, and resuspended in sterile Tris Ammonia Chloride buffer, buffered to pH 7.65. Tumour cell pellets were incubated at 37˚C for 5 min, rinsed and spun-pelleted multiple times in phosphate-buffered saline (PBS) and then plated in RPMI tissue culture media supplemented with 10% fetal calf serum (FCS), 1% L-glutamine and 1% penicillin/streptamycin/gentamycin. The cells were propagated under routine tissue culture conditions and ~50% resulted in an established cell line over ~8 weeks. The TH-*MYCN* cell lines established were validated as tyrosine hydroxylase-positive by RT-PCR (>95% positive) and had surface expression of the GD_2 disialoganglioside, as detected by flow cytometry. The control murine cell lines used were *Trp53* wild-type (wt) $MEF^{PARP-/-}$ obtained from Dr Gilbert de Murcia (18) and NIH3T3 cells. The control human neuroblastoma cell lines used were *TP53* mutant, *MYCN*-amplified SK-N-BE(2)-C, and *TP53* wt non-*MYCN*-amplified SHSY5Y [obtained from Professor Penny Lovat (Newcastle University, Newcastle upon Tyne, UK) and Dr June Biedler (Memorial Sloan Kettering Cancer Center, New York, NY, USA) and authenticated by multiplex short tandem repeat profiling by NewGene Ltd. (Newcastle upon Tyne, UK) using the GenePrint® 10 system] and *TP53* wt *MYCN*-amplified NGP cells (19). The NHO2A cells were cultured as previously described (5). The $844^{MYCN+/+}$, $282^{MYCN+/-}$, SHSY5Y, SK-N-BE(2)-C and NGP cells were cultured in RPMI-1640 (Sigma-Aldrich, Irvine, UK) supplemented with 10% fetal calf serum (FCS) (Gibco, Paisley, Scotland) and the $3261^{MYCN+/+}$, $3394^{MYCN+/+}$ and $3399^{MYCN+/+}$ cells were cultured in RPMI-1640 supplemented with 20% FCS. $MEF^{PARP-/-}$ and NIH3T3 cells were cultured in Dulbecco's modified Eagle's medium (Sigma-Aldrich) supplemented with 10% FCS.

Trp53 sequencing. DNA was extracted from tumours and cell lines using a DNeasy Blood and Tissue kit (Qiagen, Manchester, UK) according to the manufacturer's instructions. DNA from NHO2A, $844^{MYCN+/+}$ and $282^{MYCN+/-}$ cells was amplified for *Trp53* exons 2-10 and sequenced in both directions by DBS genomics (Durham University, Durham, UK). The primer sequences are available upon request. The $3261^{MYCN+/+}$, $3394^{MYCN+/+}$ and $3399^{MYCN+/+}$ DNA samples were amplified and sequenced in both directions for *Trp53* exons 5-10 by LGC Genomics GmbH (Berlin, Germany).

MDM2 inhibitors, IR, western blot analysis and flow cytometry. In brief, RG7388 was provided by Hoffman-La Roche (Nutley, NJ, USA), Nutlin-3 was purchased from Cambridge Bioscience Ltd. (Cambridge, UK) and MI-63 and NDD0005 were synthesised as previously described (20,21). The cells were irradiated using a RS320 irradiator (Gulmay Medical, Surrey, UK). For protein analysis, whole cell lysates were harvested and proteins separated using 4-20% Mini-Protean TGX Precast Gels (Bio-Rad Laboratories Ltd., Hemel Hempstead, UK) and transferred onto Hybond-C Extra membrane prior to incubation with antibodies and detection using enhanced chemiluminescence (both from GE Healthcare Life Sciences, Little Chalfont, UK) and X-ray film (Fujifilm, Bedford, UK). The primary antibodies used were p53 (1:1,000; CM5; Leica Microsystems Ltd., Buckinghamshire, UK), *MYCN* (1:100; NCMII00; Merck Millipore, Billerica, MA, USA), $p21^{WAF1}$ (1:1,000; SX118; BD Biosciences, San Jose, CA, USA), Mdm2 1:500 (2A10), $p19^{ARF}$ 1:500 (ab80) (both from Abcam, Cambridge, MA, USA) and glyceraldehyde 3-phosphate dehydrogenase (GAPDH) 1:500 (FL335; Santa Cruz Biotechnology, Inc., Dallas, TX, USA). Cell growth inhibition was determined using the XTT cell proliferation assay (Roche, Burgess Hill, UK). The cells were seeded in 96-well plates (Corning, VWR International Ltd., Lutterworth, UK), allowed to adhere overnight prior to treatment with MDM2-p53 antagonists for 48 h. For flow cytometry analysis, cells were fixed in ice-cold 70% (v/v) ethanol, and stained with

50 μg/ml propidium iodide and 50 μg/ml RNAse A (both from Sigma-Aldrich) at 37˚C for 30 min prior to analysis on the FACSCalibur (Becton-Dickinson, Oxford, UK). Data were analysed using Cyflogic (CyFlo Ltd., Turku, Finland).

Statistical analyses. Two-sided unpaired t-tests were performed using GraphPad Prism v6.0 software with a value of $P<0.05$ considered as the level of significance.

Results

Trp53 status of TH-MYCN cell lines. All TH-*MYCN* transgenic cell lines used in the present study were cultured as adherent monolayers (Fig. 1A). *Trp53* Sanger sequencing identified that 3/6 cell lines, the NHO2A, $844^{MYCN+/+}$ and $282^{MYCN+/-}$ cells, had missense coding region point mutations (Fig. 1B-D). The NHO2A cells were homozygous for a p.F106S (phenylalanine to serine; c.317 C>T) *Trp53* mutation corresponding to the human p.F109S *TP53* missense mutation (Fig. 1B). The $844^{MYCN+/+}$ cells were *Trp53* homozygous mutant for a p.C173W (cysteine to tryptophan; c.519 C>G) mutation corresponding to the human p.C176W missense mutation (Fig. 1C). Of note, the $282^{MYCN+/-}$ cells were heterozygously mutated for the same *Trp53* p.C173W mutant allele as the $844^{MYCN+/+}$ cells (Fig. 1D). Both p.F106S and p.C173W mutations are within the DNA binding domain and were predicted to affect p53-mediated transactivation using the *TP53*Mutload database. The homozygous mutations detected in NHO2A and $844^{MYCN+/+}$ cells are most likely to be due to allelic loss of one allele with mutation in the remaining allele.

To determine whether the mutations present in cell lines were also present in the original tumours or selected for during establishment of the cell line, tumour DNA was sequenced for *Trp53* exons 2-10. Only 1/6 cell lines (NHO2A) had tumour DNA available and was found to be wt (Fig. 1E).

MYCN and the p53 pathway in TH-MYCN cell lines. Basal expression of MYCN and p53 pathway components, namely p53, Mdm2, $p21^{WAF1}$ and $p19^{ARF}$ were assessed in TH-*MYCN* cell lines by western blot analysis (Fig. 1F). The *Trp53* wt murine $MEF^{PARP-/-}$ and NIH3T3, and human *MYCN* amplified *TP53* mutant SK-N-BE(2)-C cells were included as controls. Overexpression of the *MYCN* transgene was observed in all TH-*MYCN* cell lines, with levels comparable to those of the *MYCN*-amplified SK-N-BE(2)-C cells. NHO2A and $844^{MYCN+/+}$ cells had the highest *MYCN* levels compared to the other TH-*MYCN* cell lines. Accumulation of p53 was observed in NHO2A, $844^{MYCN+/+}$ and $282^{MYCN+/-}$ cells, consistent with their mutant *Trp53* status. All mouse cell lines had very low or undetectable baseline Mdm2 expression (Fig. 1F). $p21^{WAF1}$ was expressed only in *Trp53* wt $3399^{MYCN+/+}$ cell line (Fig. 1F). $p19^{ARF}$ was expressed in NHO2A, $844^{MYCN+/+}$, $3394^{MYCN+/+}$ and $3399^{MYCN+/+}$ cells (Fig. 1F).

The response of the p53 pathway to Nutlin-3 and IR. Using Nutlin-3 and IR as different methods to induce p53 activation, activation of the p53 signalling pathway was assessed by western blot analysis in the TH-*MYCN* cell lines and control *Trp53* wt $MEF^{PARP-/-}$ cells (Figs. 2 and 3). Consistent with their *Trp53* wt status, $MEF^{PARP-/-}$ cells exhibited an intact p53 signalling pathway in response to both Nutlin-3 and IR, evident by p53 stabilisation and Mdm2 and $p21^{WAF1}$ upregulation (Figs. 2A and 3A). Of note, the p53 pathway response of $MEF^{PARP-/-}$ cells to IR was slightly diminished and delayed in comparison to Nutlin-3 (Figs. 2A and 3A), and is most likely a consequence of PARP-1 knockout in this cell line (22). As expected, homozygously *Trp53* mutant NHO2A and $844^{MYCN+/+}$ cells failed to show p53 induction in response to Nutlin-3 (Fig. 2B and C) or IR (Fig. 3B and C). Consistent with this observation, no $p21^{WAF1}$ induction was observed in either cell line, and no Mdm2 induction was observed in $844^{MYCN+/+}$ cells. Of note, despite a lack of p53 induction, weak induction of Mdm2 was observed in NHO2A cells following both treatment with Nutlin-3 and exposure to IR (Figs. 2B and 3B). The heterozygously *Trp53* mutant $282^{MYCN+/-}$ cells also failed to show p53 stabilisation in response to Nutlin-3 or IR; however in spite of this, an increase in both Mdm2 and $p21^{WAF1}$ expression was observed (Figs. 2D and 3D), most likely as a result of the presence of one remaining wt *Trp53* allele. Finally, in line with their *Trp53* wt status, the 3 remaining TH-*MYCN* cell lines, $3261^{MYCN+/+}$, $3394^{MYCN+/+}$ and $3399^{MYCN+/+}$, all showed evidence of IR- and Nutlin-3-induced p53 pathway activation, with stabilisation of p53, and induction of p21 and Mdm2 (Figs. 2E-G and 3E-G).

Nutlin-3-induced cell cycle distribution. To further characterise the p53 functional response in the TH-*MYCN* cell lines to Nutlin-3, the sub-G_1 and cell cycle distribution of all the 6 TH-*MYCN* cell lines following 24 h treatment with 20 μM Nutlin-3 were analysed by propidium iodide-based flow cytometry. Sub-G_1 events was used as a surrogate marker of apoptosis and the G_1:S ratio calculated as an indicator of G_1 cell cycle arrest. *Trp53* wt NIH3T3 and $MEF^{PARP-/-}$ cells were included as positive controls. The functional assessment of Nutlin-3-mediated cell cycle arrest and apoptosis of human neuroblastoma cell lines have previously been reported (23,24). In response to Nutlin-3 treatment, NIH3T3 cells underwent G_1 arrest, evident by a 4.6-fold increase in their G1/S ratio [16.58±4.43 (Nutlin-3) vs. 3.61±0.17 (DMSO)] (Table I and Fig. 4A). Consistent with the observed activation of the p53 pathway in Fig. 2A, the $MEF^{PARP-/-}$ cells demonstrated a 3.2-fold increase in their G_1:S ratio [7.19±3.32 (Nutlin-3) vs. 2.23±0.23 (DMSO)], and a significant increase in the percentage of cells in G_2/M phase [53.32%±4.19 (Nutlin-3) vs. 34.75%±1.63 (DMSO); $P<0.005$, paired t-test] (Table I and Fig. 4A), indicative of a Nutlin-3-induced G_1 and particularly G_2 arrest in this cell line. In contrast to control *Trp53* wt murine cell lines, and as expected, no noticeable changes in the G_1/S ratio or percentage of cells in G_2/M phase were observed in any *Trp53* mutant TH-*MYCN* NHO2A, $844^{MYCN+/+}$ or $282^{MYCN+/-}$ cells (Table I and Fig. 4A). Of note, compared to the other murine cell lines, NHO2A and $282^{MYCN+/-}$ cells had a high proportion of sub-G_1 basal events (Table I and Fig. 4A), a surrogate marker of apoptosis, which following Nutlin-3 treatment, increased slightly and remained unaltered, respectively. Consistent with their *Trp53* wt status and observed p53 pathway activation, as shown in Fig. 2E-G, the 3 *Trp53* wt TH-*MYCN* cell lines, $3261^{MYCN+/+}$, $3394^{MYCN+/+}$ and $3399^{MYCN+/+}$, all underwent a G_1 phase arrest, as evident by a 5.2-, 5- and 3.4-fold increase in G_1/S ratio compared to control cells,

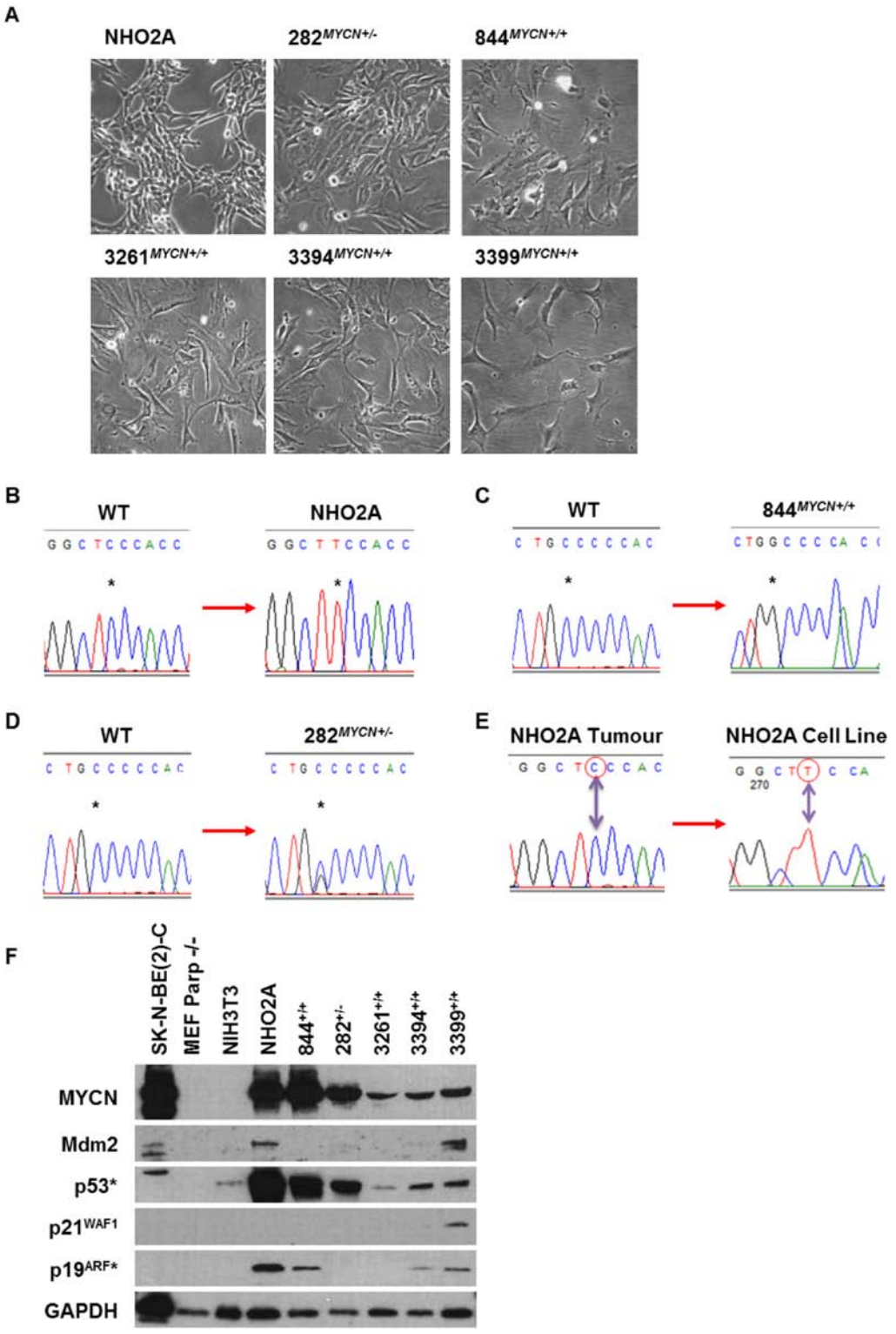

Figure 1. (A) Photomicrographs showing the morphological appearance of NHO2A, $282^{MYCN+/-}$, $844^{MYCN+/+}$, $3261^{MYCN+/+}$, $3394^{MYCN+/+}$ and $3399^{MYCN+/+}$ TH-*MYCN* murine neuroblastoma cell lines. Chromatograms showing *Trp53* gene mutations identified in (B) NHO2A (homozygous mutation, codon 106, phenylalanine to serine), (C) $844^{MYCN+/+}$ (homozygous mutation, codon 173, cysteine to tryptophan) and (D) $282^{MYCN+/-}$ (heterozygous mutation, codon 173, cysteine to tryptophan). All mutations are within the DNA binding domain of p53. The asterisk (*) marks the nucleotide change. (E) Chromatograms showing the *Trp53* wild-type (wt) status of the original tumour from which the NHO2A cell line was derived compared to the homozygous p.F106S (c.317C>T) mutation identified in the NHO2A cell line. (F) Western blot analysis of the basal expression of MYCN, Mdm2, p53, $p21^{WAF1}$ and $p19^{ARF}$ (murine homologue of $p14^{ARF}$) in the murine cell line panel in comparison to the *TP53* mutant *MYCN* amplified SK-N-BE(2)-C human neuroblastoma cell line. *p53 and $p19^{ARF}$ antibodies are only reactive against murine p53 and $p19^{ARF}$.

respectively (Table I and Fig. 4A). In addition, the $3399^{MYCN+/+}$ cells also exhibited an increased sub-G_1 population (Table I and Fig. 4A).

Species-dependent MDM2 inhibitor selectivity. MDM2 inhibitors are currently under preclinical and clinical evaluation as a novel therapeutic for neuroblastoma. To further evaluate

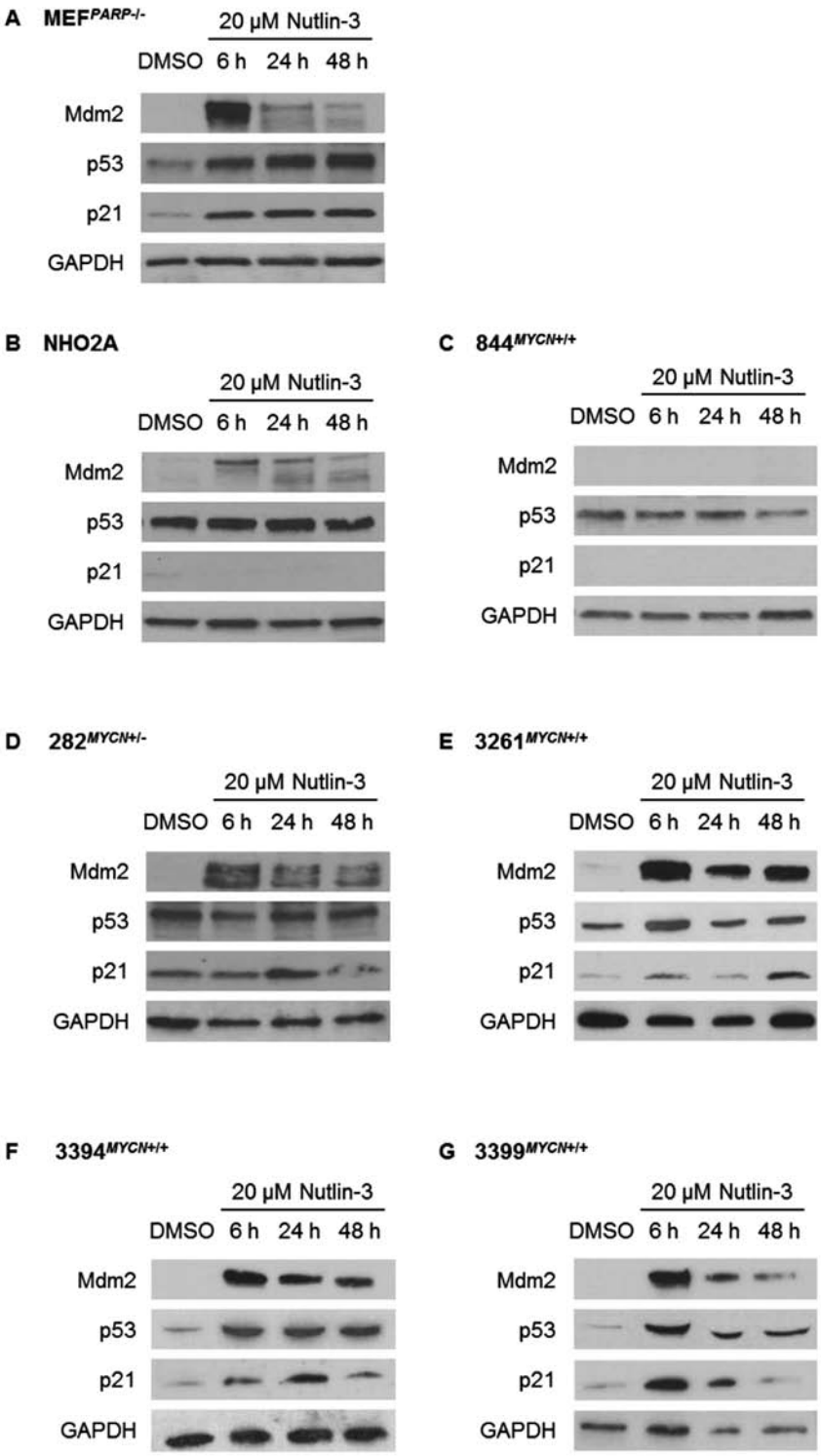

Figure 2. The response of the p53 pathway of the MEF$^{PARP-/-}$ and TH-*MYCN* transgenic murine cell lines to the MDM2 inhibitor, Nutlin-3. Western blot analysis showing levels of p53 and p53 target genes, Mdm2 and p21^{WAF1} in (A) MEF$^{PARP-/-}$, (B) NHO2A, (C) 844$^{MYCN+/+}$, (D) 282$^{MYCN+/-}$, (E) 3261$^{MYCN+/+}$, (F) 3394$^{MYCN+/+}$ and (G) 3399$^{MYCN+/+}$ cells after 6, 24 and 48 h of treatment with 20 μM Nutlin-3. Control cells were treated with either media alone (M) or media containing an equal volume of DMSO (DMSO).

the p53 pathway status of cell lines studied and establish their response to MDM2 inhibitors, sensitivity to Nutlin-3 and additional structurally unrelated MDM2 inhibitors, NDD0005, MI-63 and RG7388, and their effects on growth inhibition were assessed (Table II). Human *TP53* wt non-*MYCN* amplified SHSY5Y and *MYCN* amplified NGP cells, which have previously been shown to be sensitive to the tested MDM2 inhibitors (20,21,23), were included as positive controls. The concentrations of Nutlin-3, MI63, NDD0005 and RG7388, which led to a 50% growth inhibition (GI_{50}) after 48 h of treatment, are shown in Table II. In comparison to *TP53* wt human neuroblastoma cells, the *Trp53* wt control and TH-*MYCN* murine cell lines were less sensitive to Nutlin-3-mediated growth inhibition, as evidenced by higher GI_{50} concentrations

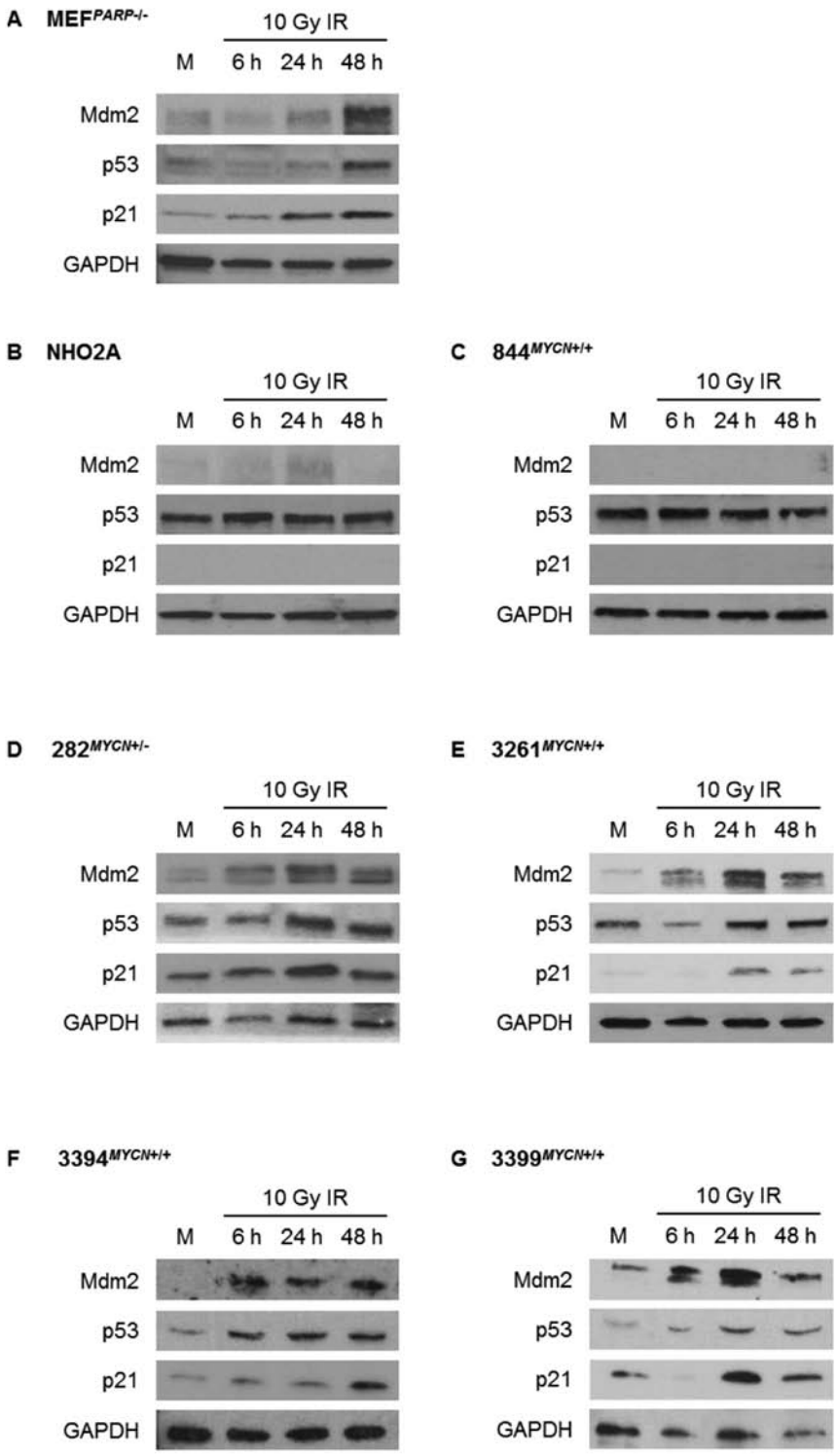

Figure 3. The p53 pathway response of MEF$^{PARP-/-}$ and TH-*MYCN* transgenic murine cell lines to ionising radiation (IR)-induced DNA damage. Western blot analysis showing the levels of p53 and p53 target genes, Mdm2 in (A) MEF$^{PARP-/-}$, (B) NHO2A, (C) 844$^{MYCN+/+}$, (D) 282$^{MYCN+/-}$, (E) 3261$^{MYCN+/+}$, (F) 3394$^{MYCN+/+}$ and (G) 3399$^{MYCN+/+}$ cells at 6, 24 and 48 h following exposure to 10 Gy IR. Control cells received no IR (M).

(1.2-7.4-fold less sensitive) (Table II and Fig. 4B). As expected, *Trp53* mutant TH-*MYCN* cell lines NHO2A, 844$^{MYCN+/+}$ and 282$^{MYCN+/-}$ had the highest GI_{50} values (14.1-21.8-fold less sensitive) (Table II).

Further evaluation and comparison of *Trp53* wt TH-*MYCN* and MEF$^{PARP-/-}$ cells to NDD0005, MI-63 and RG7388, demonstrated that although the MEF$^{PARP-/-}$ cells were significantly (2.5-3.6-fold) less sensitive to NDD0005, there was no difference in the sensitivity of *Trp53* wt TH-*MYCN* cell lines to NDD0005 compared with human SHSY5Y and NGP neuroblastoma cells (Table II and Fig. 4C). Of the tested MDM2 inhibitors, MI-63 and RG7388 were the most potent against human neuroblastoma cell lines, consistent with the findings of our previous studies (20,23). The data also revealed that compared with SHSY5Y and NGP cells, *Trp53* wt MEF$^{PARP-/-}$ cells were significantly (11.3-15.4- and 11.9-15.0-fold) less

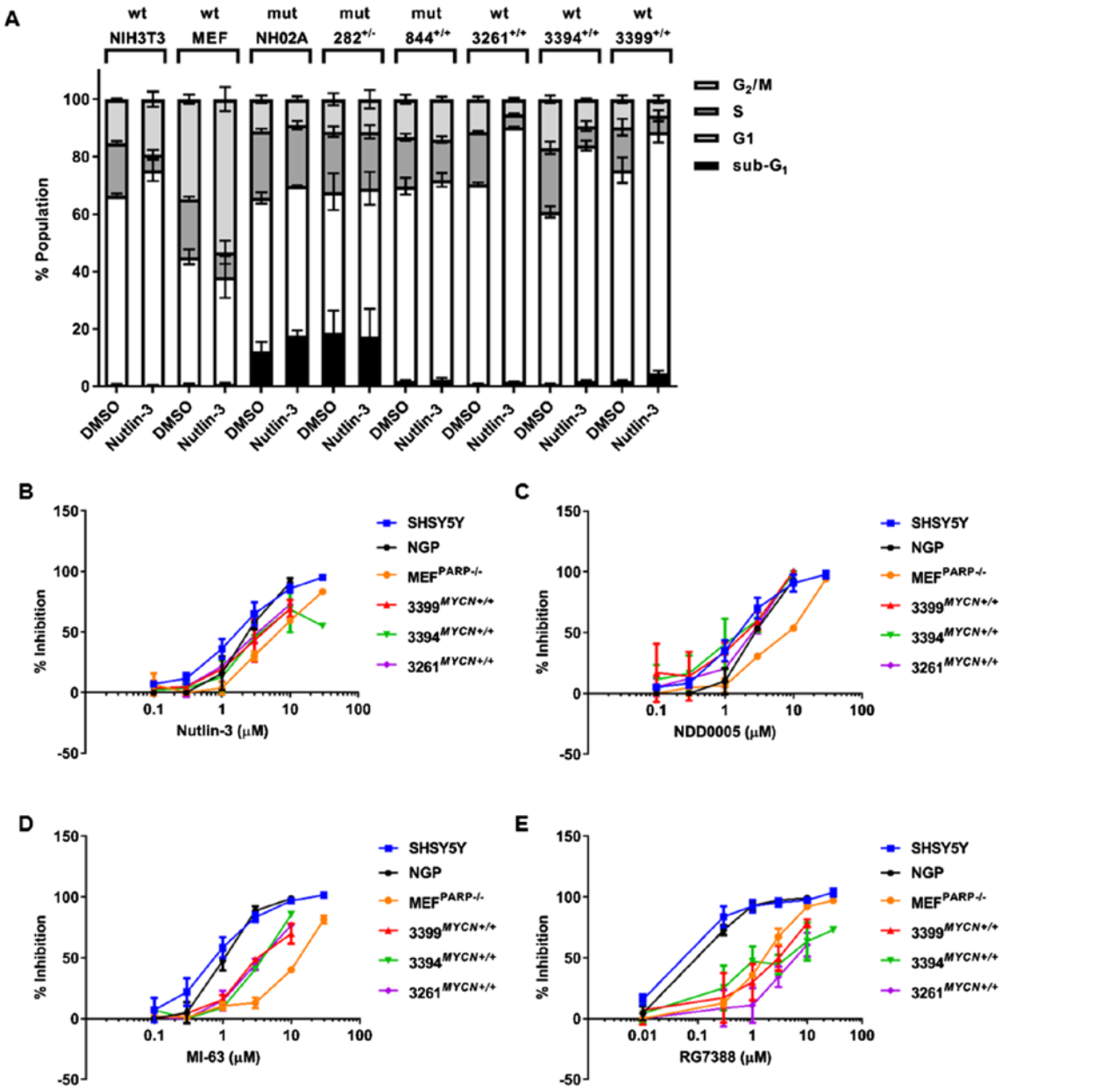

Figure 4. Cell cycle distribution and sensitivity of murine cell lines in response to Nutlin-3. (A) Graph showing the cell cycle distribution of *Trp53* wild-type (wt) murine control cells NIH3T3 and MEF$^{PARP-/-}$, and the 6 TH-*MYCN* cell lines after 24 h of treatment with 20 μM Nutlin-3. Control cells were treated with media containing an equal volume of DMSO (DMSO). Error bars represent the SEM for n=3 repeat experiments. wt, *Trp53* wt; mut, *Trp53* mutant. Dose-response growth inhibition curves for p53 wt human SHSY5Y and NGP, murine MEF$^{PARP-/-}$ and TH-*MYCN* 3261$^{MYCN+/+}$, 3394$^{MYCN+/+}$ and 3399$^{MYCN+/+}$ cells in response to 48 h treatment with (B) Nutlin-3, (C) NDD0005, (D) MI-63 and (E) RG7388.

sensitive to both MI-63 and RG7388, respectively (Table II and Fig. 4D and E). Furthermore, the data also indicated that *Trp53* wt TH-*MYCN* cell lines were significantly (3.5-5.1-fold) less sensitive to MI-63 (Table II and Fig. 4D), and even less so (13.6-59.1-fold) to RG7388 (Table II and Fig. 4E). This highlights an inverse association between potency in *TP53* wt human neuroblastoma cells and potency in *Trp53* wt murine cells.

Discussion

Cell lines established from primary tumours resected from TH-*MYCN* mice have been used to develop valuable preclinical immunocompetent, syngeneic models of neuroblastoma (7,8), for which knowledge of their p53 pathway status is important. In this study, we demonstrated that 2/6 TH-*MYCN* cell lines were *Trp53* homozygous mutant (NHO2A and 844$^{MYCN+/+}$) and 1/6 was heterozygous mutant (282$^{MYCN+/-}$). In the only case where DNA from the original tumour was available (NHO2A), the original tumour was *Trp53* wt. This is consistent with our previous analysis of 13 primary TH-*MYCN* tumours, which did not show any *Trp53* mutations (exons 4-8) (25). It is possible that *Trp53* mutant subpopulations existed within the primary tumour, but were below the level of detection of Sanger sequencing, or that the mutation spontaneously developed and was selected for during *ex vivo* culturing pressures and cell line establishment. A *MYCN* oncogenic drive may be a strong contributing factor for the positive selection of *Trp53* mutations

Table I. Flow cytometric analysis of the proportion of cells in Sub-G_1, G_1, S, and G_2/M phase, and the G_1/S ratios in the panel cell lines used in this study.

Cell line and *Trp53* status	Treatment condition	% Cell population in each phase				
		Sub-G_1	G_1	S	G_2/M	G_1/S ratio
$MEF^{PARP-/-}$	DMSO	0.66±0.37	44.46±2.57	20.13±0.89	34.75± 1.63	2.23±0.23
(wt)	Nutlin-3	0.86±0.31	37.29±7.29	8.52±4.03	53.32±4.19	7.19± 3.32
NIH3T3	DMSO	0.58±0.28	65.84±0.7	18.31±0.70	15.27±0.26	3.61±0.17
(wt)	Nutlin-3	0.39±0.17	74.89±3.73	5.37±1.64	19.34±2.68	16.58±4.43
NHO2A	DMSO	12.29± 3.2	53.35±1.98	23.28±0.79	11.07±1.33	2.29±0.01
(mutant)	Nutlin-3	17.76± 1.68	52.06±0.23	21.14±1.44	9.04±0.94	2.48±0.15
$282^{MYCN+/-}$	DMSO	18.60±7.73	49.16±6.4	20.95±1.81	11.28±2.12	2.4±0.41
(mutant)	Nutlin-3	17.37±9.66	51.58±5.73	19.69±2.29	11.37±3.22	2.68±0.41
$844^{MYCN+/+}$	DMSO	1.91±0.23	67.80±2.88	17.09±1.16	13.18±1.59	4.03±0.45
(mutant)	Nutlin-3	2.44±0.58	69.50±2.4	13.96±1.20	14.10±0.92	5.09±0.64
$3261^{MYCN+/+}$	DMSO	0.86± 0.09	69.45±0.65	18.28±0.32	11.40±0.87	3.8±0.03
(wt)	Nutlin-3	1.58± 0.05	88.61±0.28	4.57±0.41	5.24±0.41	19.67±1.68
$3394^{MYCN+/+}$	DMSO	0.91±0.16	59.88±1.98	22.28±2.12	16.94± 1.31	2.79±0.38
(wt)	Nutlin-3	1.86±0.36	82.01±1.72	6.82±1.68	9.31± 1.39	14.03±2.82
$3399^{MYCN+/+}$	DMSO	1.80±0.37	73.46±4.43	14.98±2.88	9.77±1.39	5.55±1.69
(wt)	Nutlin-3	4.63±0.97	83.93±3.61	5.76±1.79	5.69±1.26	18.67±7.01

Cell cycle analysis was performed using *Trp53* wild-type (wt) and mutant murine cell lines after 24 h of treatment with 20 μM Nutlin-3 or an equal volume of DMSO. Values represent the mean of n=3 ± SEM.

and may account for why 3/6 TH-*MYCN* cell lines tested in the present study were either homozygous or heterozygous *Trp53* mutant. Certainly, *MYCN* is known to play a dual role in driving both proliferation and apoptosis, and there are several lines of evidence, including studies using TH-*MYCN* models, which suggest that *MYCN* driven p53-dependent apoptosis is an important mechanism for tumour suppression in neuroblastoma and that *MYCN* amplified neuroblastoma cells may circumvent *MYCN* driven p53-dependent apoptosis by selecting for cells with aberrations in the p53/MDM2/$p14^{ARF}$ pathway, as has been observed for MYCC-driven lymphoma (3,19,26-29). Specifically, as previously demonstrated, tumours formed with greater penetrance and reduced latency in TH-*MYCN* mice heterozygous for an inactivated germline p53 allele (27). The analysis of human neuroblastoma cell lines reported to date with aberrations in the p53/MDM2/$p14^{ARF}$ pathway demonstrates that 31/40 (78%) are *MYCN*-amplified (19). More recently, a study of the role of p53 function in neuroblastoma pathogenesis using TH-*MYCN* murine models observed that loss of p53 function led to reduced survival (30).

Nutlin-3 is a potent selective inhibitor of the MDM2-p53 interaction (31), previously shown to be highly effective against *TP53* wt neuroblastoma cell lines, inducing cell cycle arrest and/or apoptosis, and used to functionally screen large neuroblastoma cell line panels for p53 pathway aberrations (23,24,32). In this study, we found that in all cell lines tested, the presence of a mutation was consistent with high basal levels of p53 and aberrant p53 signalling in response to Nutlin-3 and IR, and failure to growth arrest in response to Nutlin-3. Consistent with the mechanisms of action of MDM2 inhibitors and existing data from human neuroblastoma cell lines, overall, Nutlin-3 was found to induce cell cycle arrest and/or apoptosis of *Trp53* wt control and TH-*MYCN* murine cell lines (23,24). Of note, in the current study, in response to Nutlin-3 and IR, although there was no induction of p53, an increase in both Mdm2 and $p21^{WAF1}$ expression was observed in heterozygously mutant $282^{MYCN+/-}$ cells, suggesting there is some residual p53 function from the remaining wt allele (33); however this did not lead to growth arrest or apoptosis in response to Nutlin-3.

MDM2 inhibitors are currently under preclinical and clinical development as a novel therapeutic, both alone and in combination, for human malignancies including neuroblastoma. Of particular interest in view of the latter, data from the present study demonstrated that in comparison to human *TP53* wt neuroblastoma cells, murine control ($MEF^{PARP-/-}$) and TH-*MYCN* cell lines were significantly less sensitive to MI-63 and RG7388 induced growth inhibition. Although human and murine MDM2 show a high degree of amino acid sequence homology, with only 2 non-identical amino acids within the p53 binding domain (34), these subtle differences could account for a weaker binding affinity to murine Mdm2 which is believed to contribute to the increased resistance and higher GI_{50} concentrations of murine cells to some MDM2 inhibitors that have been designed with high potency against human MDM2 (35). In support of this, the present

Table II. Summary of 48-h GI_{50} values for MDM2 antagonists in human and murine cells.

Cell line	48 h	Antagonist (μM)			
		Nutlin-3	NDD0005	MI-63	RG7388
SHSY5Y	GI_{50}	1.95±0.56	1.93±0.69	0.78±0.16	0.11±0.05
NGP	GI_{50}	2.51±0.3	2.78±0.02	1.06±0.12	0.14±0.03
MEF$^{PARP-/-}$	GI_{50}	7.10±0.38	6.98±0.06	12.05±0.63	1.61±0.11
	Rel Fold/P-value vs. SHSY5Y	3.6/[b]	3.6/[b]	15.4/[d]	15.0/[d]
	Rel Fold/P-value vs. NGP	2.8/[b]	2.5/[c]	11.3/[c]	11.9/[c]
NIH3T3	GI_{50}	14.1±2.2	ND	ND	ND
	Rel Fold/P-value vs. SHSY5Y	7.4/[b]			
	Rel Fold/P-value vs. NGP	5.6/[b]			
NHO2A	GI_{50}	41.4±2.7	ND	ND	ND
	Rel Fold/P-value vs. SHSY5Y	21.8/[d]			
	Rel Fold/P-value vs. NGP	16.5/[d]			
282$^{MYCN+/-}$	GI_{50}	35.3±1.8	ND	ND	ND
	Rel Fold/P-value vs. SHSY5Y	18.6/[d]			
	Rel Fold/P-value vs. NGP	14.1/[d]			
844$^{MYCN+/+}$	GI_{50}	36.5±1.4	ND	ND	ND
	Rel Fold/P-value vs. SHSY5Y	19.2/[d]			
	Rel Fold/P-value vs. NGP	14.5/[d]			
3261$^{MYCN+/+}$	GI_{50}	3.53±0.54	2.38±0.39	3.71±0.3	6.36±1.65
	Rel Fold/P-value vs. SHSY5Y	1.8/ns	1.2/ns	4.7/[c]	59.1/[b]
	Rel Fold/P-value vs. NGP	1.4/ns	0.9/ns	3.5/[b]	47.0/[a]
3394$^{MYCN+/+}$	GI_{50}	3.09±0.19	1.57±0.63	4.0±0.41	1.84±0.50
	Rel Fold/P-value vs. SHSY5Y	1.6/ns	0.8/ns	5.1/[c]	17.1/[b]
	Rel Fold/P-value vs. NGP	1.2/ns	0.6/ns	3.8/[b]	13.6/[a]
3399$^{MYCN+/+}$	GI_{50}	4.3±1.2	1.58±0.65	3.94±0.58	3.49±0.37
	Rel Fold/P-value vs. SHSY5Y	2.2/ns	0.8/ns	5/[b]	32.4/[c]
	Rel Fold/P-value vs. NGP	1.7/ns	0.6/ns	3.7/[b]	25.8/[b]

Values represent the means ± SEM. P-values were determined using unpaired t-tests vs. human neuroblastoma SHSY5Y or NGP cells, [a]P≤0.05; [b]P≤0.01; [c]P≤0.001; [d]P≤0.0001; ns, not statistically significant. Rel Fold, fold change relative to the GI_{50} value of SHSY5Y cells and the GI_{50} value of NGP cells; vs., versus; ND, not determined.

data showed that the more potent the MDM2 inhibitor was against human neuroblastoma cells, the less sensitive the murine cells were, and the greater the fold difference between GI_{50} values of *Trp53* wt murine cells vs. *TP53* wt human cells. These observations are consistent with the inter-species selectivity of spiro-oxindole-based MDM2 inhibitors (36) and dihydroisoquinolinone NVP-CGM097 (37), but not pyrazolo-pyrrolidinone NVP-HDM201 (38,39), and should be taken into account when designing studies of MDM2 inhibitors either alone or in combination using either preclinical transgenic or human tumour xenograft models as p53-dependent normal tissue toxicity will not be adequately modelled.

Currently, murine neuroblastoma models include genetically engineered mouse models, syngeneic models, and subcutaneous, orthotopic, pseudometastatic and patient-derived xenografts (3,40-43). All models have associated advantages and disadvantages, and it is likely that the most comprehensive preclinical assessment of efficacy will include a combination of existing models. Several of the models predominantly use immunocompromised mice and thus are unsuitable for assessment of immunotherapies, which are emerging as effective targeted therapies in patients with neuroblastoma. To overcome this, cell lines established from the TH-*MYCN* transgenic model/or other murine neuroblastoma cell lines can be used to generate orthotopic or pseudometastatic syngeneic models of neuroblastoma in an immunocompetent background (7,8). For this, the genetic and functional characterisation of murine cell lines, including *Trp53* status and pathway function, are very important and highly warranted, as existing data are limited.

In conclusion, the *Trp53* wt and mutant TH-*MYCN* cell lines characterised in this study can be used in syngeneic models of neuroblastoma, the former to test p53-dependent therapies in combination with immunotherapies, such as anti-GD_2 antibody, and the latter as models of immunocompetent, chemoresistant relapsed neuroblastoma in which aberrations in the p53 pathway are more common (14-16).

Acknowledgements

This study was supported by The Dubois Child Cancer Fund, SPARKS, the North of England Children's Cancer Research Fund (NECCRF), Neuroblastoma UK and Niamh's Next Step. We would like to thank Professor Michelle Haber for the NHO2A cell line and tumour DNA, Dr Gilbert de Murcia for providing the MEF$^{PARP-/-}$ cells, Dr Fabio Del Bello and Dr Alessandro Piergentili for providing MI-63, Dr Steven Middleton (Hoffmann-La Roche, Nutley, NJ, USA) for providing RG7388, and Dr Anna Watson, Dr Karen Haggerty and Dr Ian Hardcastle (Newcastle University) for synthesising NDD0005. We disclose that Dr L. Chen and Professor D.A. Tweddle are part of an international collaborative research consortium with Hoffmann-La Roche Ltd. Professor J. Lunec is a collaborative co-investigator of the CRUK funded Drug Discovery Programme at Newcastle University which developed NDD0005. Newcastle University, Cancer Research Technology and Astex Pharmaceuticals Inc. are part of an alliance agreement since 2012.

Competing interests

The authors declare that they have no competing interests.

References

1. Cohn SL and Tweddle DA: MYCN amplification remains prognostically strong 20 years after its 'clinical debut'. Eur J Cancer 40: 2639-2642, 2004.
2. Weiss WA, Aldape K, Mohapatra G, Feuerstein BG and Bishop JM: Targeted expression of MYCN causes neuroblastoma in transgenic mice. EMBO J 16: 2985-2995, 1997.
3. Chesler L and Weiss WA: Genetically engineered murine models - contribution to our understanding of the genetics, molecular pathology and therapeutic targeting of neuroblastoma. Semin Cancer Biol 21: 245-255, 2011.
4. Rasmuson A, Segerström L, Nethander M, Finnman J, Elfman LH, Javanmardi N, Nilsson S, Johnsen JI, Martinsson T and Kogner P: Tumor development, growth characteristics and spectrum of genetic aberrations in the TH-MYCN mouse model of neuroblastoma. PLoS One 7: e51297, 2012.
5. Cheng AJ, Cheng NC, Ford J, Smith J, Murray JE, Flemming C, Lastowska M, Jackson MS, Hackett CS, Weiss WA, *et al*: Cell lines from MYCN transgenic murine tumours reflect the molecular and biological characteristics of human neuroblastoma. Eur J Cancer 43: 1467-1475, 2007.
6. Lehembre F and Regenass U: Metastatic disease: A drug discovery perspective. Semin Cancer Biol 22: 261-271, 2012.
7. Stauffer JK, Orentas RJ, Lincoln E, Khan T, Salcedo R, Hixon JA, Back TC, Wei JS, Patidar R, Song Y, *et al*: High-throughput molecular and histopathologic profiling of tumor tissue in a novel transplantable model of murine neuroblastoma: New tools for pediatric drug discovery. Cancer Invest 30: 343-363, 2012.
8. Kroesen M, Nierkens S, Ansems M, Wassink M, Orentas RJ, Boon L, den Brok MH, Hoogerbrugge PM and Adema GJ: A transplantable TH-MYCN transgenic tumor model in C57Bl/6 mice for preclinical immunological studies in neuroblastoma. Int J Cancer 134: 1335-1345, 2014.
9. Brown CJ, Lain S, Verma CS, Fersht AR and Lane DP: Awakening guardian angels: drugging the p53 pathway. Nature reviews 9: 862-873, 2009. https://doi.org/10.1038/nrc2763.
10. Carr J, Bell E, Pearson ADJ, Kees UR, Beris H, Lunec J and Tweddle DA: Increased frequency of aberrations in the p53/MDM2/p14(ARF) pathway in neuroblastoma cell lines established at relapse. Cancer Res 66: 2138-2145, 2006.
11. Keshelava N, Zuo JJ, Chen P, Waidyaratne SN, Luna MC, Gomer CJ, Triche TJ and Reynolds CP: Loss of p53 function confers high-level multidrug resistance in neuroblastoma cell lines. Cancer Res 61: 6185-6193, 2001.
12. Levine AJ: p53, the cellular gatekeeper for growth and division. Cell 88: 323-331, 1997.
13. Soussi T and Béroud C: Assessing TP53 status in human tumours to evaluate clinical outcome. Nat Rev Cancer 1: 233-240, 2001.
14. Carr-Wilkinson J, O'Toole K, Wood KM, Challen CC, Baker AG, Board JR, Evans L, Cole M, Cheung NK, Boos J, *et al*: High Frequency of p53/MDM2/p14^{ARF} Pathway Abnormalities in Relapsed Neuroblastoma. Clin Cancer Res 16: 1108-1118, 2010.
15. Tweddle DA, Malcolm AJ, Bown N, Pearson AD and Lunec J: Evidence for the development of p53 mutations after cytotoxic therapy in a neuroblastoma cell line. Cancer Res 61: 8-13, 2001.
16. Padovan-Merhar OM, Raman P, Ostrovnaya I, Kalletla K, Rubnitz KR, Sanford EM, Ali SM, Miller VA, Mossé YP, Granger MP, *et al*: Enrichment of targetable mutations in the relapsed neuroblastoma genome. PLoS Genet 12: e1006501, 2016.
17. Evageliou NF, Haber M, Vu A, Laetsch TW, Murray J, Gamble LD, Cheng NC, Liu K, Reese M, Corrigan KA, *et al*: Polyamine antagonist therapies inhibit neuroblastoma initiation and progression. Clin Cancer Res 22: 4391-4404, 2016.
18. de Murcia JM, Niedergang C, Trucco C, Ricoul M, Dutrillaux B, Mark M, Oliver FJ, Masson M, Dierich A, LeMeur M, *et al*: Requirement of poly(ADP-ribose) polymerase in recovery from DNA damage in mice and in cells. Proc Natl Acad Sci USA 94: 7303-7307, 1997.
19. Chen L and Tweddle DA: p53, SKP2, and DKK3 as MYCN target genes and their potential therapeutic significance. Front Oncol 2: 173, 2012.
20. Chen L, Zhao Y, Halliday GC, Berry P, Rousseau RF, Middleton SA, Nichols GL, Del Bello F, Piergentili A, Newell DR, *et al*: Structurally diverse MDM2-p53 antagonists act as modulators of MDR-1 function in neuroblastoma. Br J Cancer 111: 716-725, 2014.
21. Chen L, Rousseau RF, Middleton SA, Nichols GL, Newell DR, Lunec J and Tweddle DA: Pre-clinical evaluation of the MDM2-p53 antagonist RG7388 alone and in combination with chemotherapy in neuroblastoma. Oncotarget 6: 10207-10221, 2015.
22. Valenzuela MT, Guerrero R, Núñez MI, Ruiz De Almodóvar JM, Sarker M, de Murcia G and Oliver FJ: PARP-1 modifies the effectiveness of p53-mediated DNA damage response. Oncogene 21: 1108-1116, 2002.
23. Gamble LD, Kees UR, Tweddle DA and Lunec J: MYCN sensitizes neuroblastoma to the MDM2-p53 antagonists Nutlin-3 and MI-63. Oncogene 31: 752-763, 2012.
24. Van Maerken T, Rihani A, Dreidax D, De Clercq S, Yigit N, Marine JC, Westermann F, De Paepe A, Vandesompele J and Speleman F: Functional analysis of the p53 pathway in neuroblastoma cells using the small-molecule MDM2 antagonist nutlin-3. Mol Cancer Ther 10: 983-993, 2011.
25. Mazanek P, Dam V, Morgan BT, Liu X, Pawar N and Hogarty MD: Assessment of p19/ARF-MDM-p53 and RAS pathways for alterations in neuroblastomas arising in the transgenic TH-MYCN mouse model. In: Advances in Neuroblastoma Research June 16-19th 2004, Genoa, Italy, 2004.
26. Chen L, Iraci N, Gherardi S, Gamble LD, Wood KM, Perini G, Lunec J and Tweddle DA: p53 is a direct transcriptional target of MYCN in neuroblastoma. Cancer Res 70: 1377-1388, 2010.
27. Chesler L, Goldenberg DD, Collins R, Grimmer M, Kim GE, Tihan T, Nguyen K, Yakovenko S, Matthay K and Weiss WA: Chemotherapy-induced apoptosis in a transgenic model of neuroblastoma proceeds through p53 induction. Neoplasia 10: 1268-1274, 2008.
28. Chen Z, Lin Y, Barbieri E, Burlingame S, Hicks J, Ludwig A and Shohet JM: Mdm2 deficiency suppresses MYCN-Driven neuroblastoma tumorigenesis in vivo. Neoplasia 11: 753-762, 2009.
29. Eischen CM, Weber JD, Roussel MF, Sherr CJ and Cleveland JL: Disruption of the ARF-Mdm2-p53 tumor suppressor pathway in Myc-induced lymphomagenesis. Genes Dev 13: 2658-2669, 1999.
30. Yogev O, Barker K, Sikka A, Almeida GS, Hallsworth A, Smith LM, Jamin Y, Ruddle R, Koers A, Webber HT, *et al*: p53 loss in MYC-driven neuroblastoma leads to metabolic adaptations supporting radioresistance. Cancer Res 76: 3025-3035, 2016.
31. Vassilev LT, Vu BT, Graves B, Carvajal D, Podlaski F, Filipovic Z, Kong N, Kammlott U, Lukacs C, Klein C, *et al*: In vivo activation of the p53 pathway by small-molecule antagonists of MDM2. Science 303: 844-848, 2004.
32. Chen L, Malcolm AJ, Wood KM, Cole M, Variend S, Cullinane C, Pearson AD, Lunec J and Tweddle DA: p53 is nuclear and functional in both undifferentiated and differentiated neuroblastoma. Cell Cycle 6: 2685-2696, 2007.

33. Sun Y, Yi H, Yang Y, Yu Y, Ouyang Y, Yang F, Xiao Z and Chen Z: Functional characterization of p53 in nasopharyngeal carcinoma by stable shRNA expression. Int J Oncol 34: 1017-1027, 2009.
34. Vassilev LT: Small-molecule antagonists of p53-MDM2 binding: research tools and potential therapeutics. Cell Cycle 3: 419-421, 2004.
35. Khoo KH, Verma CS and Lane DP: Drugging the p53 pathway: Understanding the route to clinical efficacy. Nat Rev Drug Discov 13: 217-236, 2014.
36. Delaisi C, Meaux I, Dos-Santos O, Barrière C, Duffieux F, Hoffmann D, Rak A, Wolfrom M, Flèche , Zhou-Liu Q, *et al*: In vitro characterization of spiro-oxindole-based modulators of the MDM2-p53 interaction and their interspecies selectivity. 103rd Annual Meeting of the American Association for Cancer Research, Mar 31-Apr 4, 2012. Cancer Res 72: Abstract nr 4648, Chicago, IL, 2012.
37. Holzer P, Masuya K, Furet P, Kallen J, Valat-Stachyra T, Ferretti S, Berghausen J, Bouisset-Leonard M, Buschmann N, Pissot-Soldermann C, *et al*: Discovery of a dihydroisoquinolinone derivative (NVP-CGM097): A highly potent and selective MDM2 inhibitor undergoing phase 1 clinical trials in p53wt tumors. J Med Chem 58: 6348-6358, 2015.
38. Stachyra-Valat T, Baysang F, D'Alessandro A-C, Dirk E, Furet P, Guagnano V, Kallen J, Leder L, Mah R, Masuya K, *et al*: Abstract 1239: NVP-HDM201: Biochemical and biophysical profile of a novel highly potent and selective PPI inhibitor of p53-Mdm2. Cancer Res 76 (Suppl 14): 1239-1239, 2016.
39. Furet P, Masuya K, Kallen J, Stachyra-Valat T, Ruetz S, Guagnano V, Holzer P, Mah R, Stutz S, Vaupel A, *et al*: Discovery of a novel class of highly potent inhibitors of the p53-MDM2 interaction by structure-based design starting from a conformational argument. Bioorg Med Chem Lett 26: 4837-4841, 2016.
40. Heukamp LC, Thor T, Schramm A, De Preter K, Kumps C, De Wilde B, Odersky A, Peifer M, Lindner S, Spruessel A, *et al*: Targeted expression of mutated ALK induces neuroblastoma in transgenic mice. Sci Transl Med 4: 141ra91, 2012.
41. Khanna C and Hunter K: Modeling metastasis in vivo. Carcinogenesis 26: 513-523, 2005.
42. Khanna C, Jaboin JJ, Drakos E, Tsokos M and Thiele CJ: Biologically relevant orthotopic neuroblastoma xenograft models: Primary adrenal tumor growth and spontaneous distant metastasis. In Vivo 16: 77-85, 2002.
43. Beltinger C and Debatin KM: Murine models for experimental therapy of pediatric solid tumors with poor prognosis. Int J Cancer 92: 313-318, 2001.